

# Radiation Effects on Fused Biconical Taper Wavelength Division Multiplexer

Roman C. Gutierrez, Gary M. Swift, Serge Dubovitsky, Randall K. Bartman,  
Charles E. Barnes, Leonard Dorsky  
Jet Propulsion Laboratory, California Institute of Technology  
4800 Oak Grove Dr., Pasadena, CA 911 09

## Abstract

The effects of radiation on fused biconical taper wavelength division multiplexers are presented. A theoretical model indicates that index changes in the fiber are primarily responsible for the degradation of these devices.

## I. INTRODUCTION

A single optical source uses only a small part of the available spectral transmission band of an optical fiber. Transmitting information at several wavelengths simultaneously through a single optical fiber will ideally multiply the transmission capability of the fiber times the number of wavelengths used. In order to combine the sources into one fiber, and separate them at the output of a fiber, wavelength division multiplexer (WDM) are required.

Several authors have studied the effect of radiation on different types of optical couplers [10,11,12,24]. In this paper, we will limit ourselves to the fused biconical tapered WDM which is made by fusing together two single mode fibers. Fused biconical taper WDMs are the most widely used type of coupler in the telecommunications industry, making them the most likely candidate for multiplexed high data-rate optical buses in space.

The severe requirements for optical WDMs (30-35 dB isolation) in most telecommunications applications are barely met by fused biconical taper WDMs (typically in concatenated structures or followed by wavelength filters) [26]. In order to use these devices in space applications, the radiation hardness of these devices needs to be studied in order to establish the effects of radiation, the mechanism responsible for the effects, and possible directions to take in the development of a radiation hardened WDM.

This paper will modify the existing theoretical analysis of fused biconical tapered couplers [17-23,26] to correct for core index of refraction and combine with known effects of radiation on optical fiber [1,2,3,4,5,25] to model the effects of radiation on these devices. In the case of fiber, the change in attenuation dominates its degradation in performance, but for WDMs it will be shown that the index change caused by the radiation is most important.

## 11. WAVELENGTH DIVISION MULTIPLEXER

Numerous articles and [15, 16, 26] discuss the advantages of wavelength multiplexing in optical systems. Much the

same as frequency multiplexing in radio and television, wavelength multiplexing increases the bandwidth of an optical system by the number of different wavelengths used. The combination and distribution of the different optical wavelengths is performed by a device called wavelength division multiplexers (WDM).

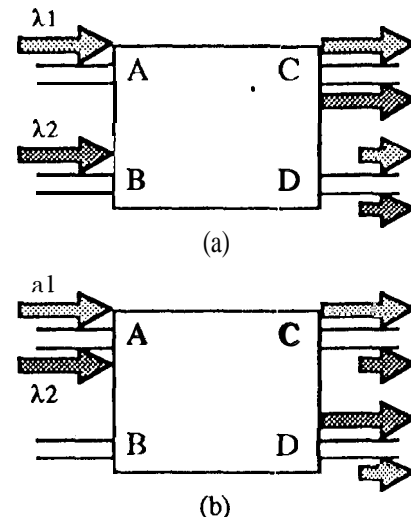


Fig. 1 A WDM operating as (a) a multiplexer (b) a demultiplexer.

A two-wavelength WDM is shown in figure 1. The device has four ports which are labeled A through D. The WDM can function either as a multiplexer (wavelength combiner) or as a demultiplexer (wavelength divider) for wavelengths that closely match  $\lambda_1$  and  $\lambda_2$ . Figure 1a shows the operation of a WDM as a multiplexer. When light at  $\lambda_1$  is injected into port A and light at  $\lambda_2$  into port B, the WDM combines the two wavelengths at port C. Port D is the crosstalk channel, and some light at both wavelengths exits through this channel. Figure 1b shows a WDM operating as a demultiplexer. When light at both wavelengths is injected into port A, the WDM separates the two wavelengths into ports C and D. The majority of light at  $\lambda_1$  exits out of port C, but some comes out through D. Light at  $\lambda_2$  is separated from light at  $\lambda_1$  mostly coming out through port D.

In order to quantify the performance of a WDM, two figures of merit are typically used. *Isolation* is defined as the ratio of the output of port D to the output of port C when light at a single wavelength is injected into port A. *Excess loss* is the ratio of the total output to the total input. These values are usually expressed in dBopt.

$$\text{isolation} = 10 \log_{10} \left( \frac{D}{C} \right) \quad (1)$$

$$\text{excess loss} = 10 \log_{10} \left( \frac{C+D}{A+B} \right) \quad (2)$$

In addition, the operating wavelength range is usually specified (typically  $\pm 20$  nm at  $\lambda_1$  and  $\lambda_2$ ).

A beam of light can be separated into its spectral components by many different methods such as using gratings or prisms. Wavelength division methods such as these have been integrated with fiber and used for wavelength division multiplexing [15,16,24], but the most successful WDM has evolved from tapered fiber technology. This type of WDM is the one treated in this paper and is described in the next section.

### III. FUSED BICONICAL TAPER WDM

#### A. Tapered optical fiber

When an optical fiber is heated above the glass softening point and stretched symmetrically, the diameter of the fiber is decreased at the heat source and gradually tapers to the original diameter away from the heat source. When light is launched into the tapered fiber, the mode in the fiber will change along the taper. Far away from the tapered region, the light in the fiber is guided by the core, and the cladding can be assumed to extend to infinity. But as the fiber gets thinner, the mode field diameter approaches the diameter of the cladding and the cladding becomes the guiding medium. If the taper is slow (adiabatic approximation) all the energy will be carried by the lowest order mode at every point in the fiber. In this case, there is no loss of energy and the presence of the taper is not detectable from the properties of the fiber. If the taper is very sudden, higher order modes will be excited as the light travels along the taper-down region and interfere when they couple into the fundamental mode of the fiber in the taper-up region. The so-called Stewart-Love limit [26] determines the slope of the taper below which only the fundamental mode carries the energy and above which higher order modes are excited.

#### B. Fused biconical taper WDM

When two fibers are heated and stretched together in such a way that the taper slope is below the Stewart-Love limit, the first two lower order modes are excited in the region between the tapers. The coupling between the two fibers is then determined by the interference between these two modes.

Figure 2 shows a fused biconical tapered coupler. The fused region is typically about 3 cm long, but the region where most of the coupling takes place (the coupling region in figure 2) is only around 5 mm long. The original core diameter and cladding diameters for SMF28 fiber (which is usually used to make these devices) are  $9 \mu\text{m}$  and  $125 \mu\text{m}$  respectively. The width of the coupling region is typically around  $30 \mu\text{m}$  but varies between individual devices.

The principal coupling mechanism in fused biconical tapered couplers is fundamentally different from polished fiber-optic WDMs or optoelectronic directional couplers which work by evanescent coupling [6,7,11,12,13]. In a fused biconical taper coupler, most of the coupling results from the interference between the first two fundamental modes in the coupling region, which can be approximated as a rectangular waveguide of constant cross-section. Only a small portion of the coupling is evanescent.

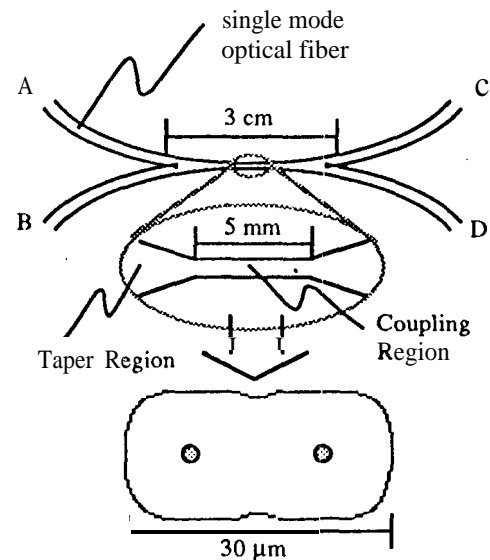


Fig. 2 A fused biconical taper WDM. Magnification and cross-section of the coupling region.

Outside the fused region, the interaction between the two fibers is small enough that any mode can be expressed as a vector sum of the fundamental modes of the two fibers. Along the taper-down region, the modes in the two fibers begin to interact becoming distorted. This interaction results in a small amount of coupling. Since the interaction between the two modes comes from the overlap of one of the modes with the evanescent field of the other mode, this type of interaction and the energy exchange between the two modes is called evanescent coupling.

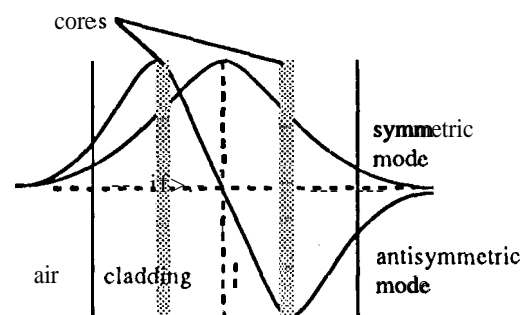


Fig. 3. Symmetric and antisymmetric modes in the coupling region.

As the mode field diameter approaches the diameter of the cladding, the cores of the fibers are no longer guiding the light, and the cladding becomes the guiding structure. Since the taper slope is below the Stewart-Love limit, only the first two fundamental modes of the cladding-air waveguide are excited. These two modes are shown in figure 3.

Since the symmetric mode is more confined to the fiber than the antisymmetric mode, the antisymmetric mode propagates faster. The difference in velocity of the two modes results in a build up of the relative phase between them as they propagate through the coupling region. As the fibers taper out, the modes adiabatically conform to the modes of the two single mode fibers forcing the symmetric and antisymmetric modes to interfere. The output of the two fibers is then determined by the interference pattern. If we ignore the phase shift between the symmetric and antisymmetric modes acquired in the tapered regions, and only consider the phase shift between the two modes in the coupling region, the coupling constant is given by:

$$C = k_A - k_S = \frac{2\pi}{\lambda} (n_A - n_S) \quad (3)$$

where  $n_A$  and  $n_S$  are the effective index of refraction of the antisymmetric mode and the effective index of refraction of the symmetric mode in the coupling region respectively.  $\lambda$  is the free space wavelength of light.

Due to the dependence on wavelength of the coupling constant ( $n_A$  and  $n_S$  are also dependent on  $\lambda$ ), fused biconical tapered couplers can be tailored to have near 100% coupling at one wavelength and near 0% coupling at a second wavelength. A coupler which is tailored in this way is called a WDM.

#### IV. EXPERIMENTAL PROCEDURE

Table 1 lists all the devices that were irradiated in the order that the irradiations were done. A description of the radiation they were exposed to is listed in the three columns labeled "RADIATION". The "where" column indicates which section of the device was irradiated. "whole" means that the entire WDM was exposed to radiation, "input" means that only a section of the WDM on the side of the input was irradiated, "output" means that a region close to the output of the WDM was exposed to radiation, "o-c" stands for output-center, and "i-c" stands for input-center. The "Type" column indicates whether the device was exposed to protons (p+) or Radioactive Cobalt ( $Co^{60}$ ). The "Dose" column indicates the total dose received by the device in Mrad ( $SiO_2$ ). The type of device tested is given in the "Device Name" column.

The ML devices were supplied by NCCOSC Research, Development, Test and Evaluation Division. These devices were bare, i.e. the taper region of the WDM was exposed to atmosphere. The devices were supplied in this way to permit low energy proton irradiation (6 MeV). A total of three of these devices were irradiated. The first one (ML-1) was exposed to 6 MeV protons at a dose rate of 1.3 krad/min for the first 100 krad, and at a dose rate of 10 krad/min for the last 900 krad. ML-2 was exposed to  $Co^{60}$  for a total dose of 1

Mrad and 6 MeV protons for 500 krad. The relaxation of the device was observed for 45 minutes after 100 krad and for 9 hours after 1 Mrad. The dose rate was 1.3 krad/min for the first 100 krad and 3 krad/min for the 900 krad. The dose rate during proton irradiation was 10 krad/min. The last of these devices (ML-3) was subjected to sectional proton irradiation (5 mm sections of the device were irradiated consecutively). The dose rate was 10 krad/min. The device was masked with a 5 mm slit in a piece of aluminum.

Device Name	RADIATION			ISOLATION (dB)			
	where	Type	Dose Mrad	$\lambda = 1.31 \mu m$ Pre-rad	$\lambda = 1.31 \mu m$ $\Delta_{rad}$	$\lambda = 1.55 \mu m$ Pre-rad	$\lambda = 1.55 \mu m$ $\Delta_{rad}$
ML-1	whole	p+	1	-19	+3	-28	+10
ML-2	"	$Co^{60}$	0.1	-24	+0.8	-23.6	+0.5
"	"	"	0.9	-23.2	+2.7	-23.1	+1.6
"	"	p+	0.5	-21.8	+1.4	-22.4	+2.2
ML-3	input	"	0.2	-27.45	0	-26.7	0
"	output	"	"	-27.5	0	-26.7	0
"	center	"	"	-27.4	-1.4	-26.7	-0.3
"	o-c	"	"	-28.6	-0.7	-26.9	-0.2
"	i-c	"	"	-29.1	-0.3	-27.1	-0.2
Gould-1	whole	"	0.1	-20.6	+0.5	-19.9	+1.1
"	"	"	0.9	-20.1	+1.7	-18.8	+2.3
Gould-2	"	$Co^{60}$	0.1	-24.4	-1.5	-24	+1.8
"	"	"	0.9	-25.8	-2.2	-22.3	+2.7
"	"	"	1	-27.44	-0.42	-20.1	+0.8
"	"	"	"	-27.84	-0.28	-18.83	+0.6
Gould-3	"	"	"	-25.7	+2.4	-25.2	+3.9
Gould-4	"	"	0.1	-24.6	+0.7	-19.2	+0.9
"	input	"	0.2	-23.9	+0.9	-18.3	+0.3
"	output	"	"	-23	+0.05	-18	0
"	center	"	"	-22.95	+0.8	-18	+0.5
"	whole	"	"	-22.15	+0.45	-17.5	+0.3
E-1 (TE)	"	"	1	-30.7	+5.6	-18.5	+2
(TM)	"	"	"	-33.2	+6	-27	+3.5

Table 1. Summary of test results.

The Gould devices were supplied by Gould Inc. Fiber-Optics Division, Gould-1 and Gould-2 are the 16 dB isolation in a 40 nm band model, and Gould-3 and Gould-4 are the 10 dB isolation in a 40 nm band model. Gould-1 was the only Gould device irradiated with protons. Since the devices were all packaged, the proton irradiation was done at the UC Davis Cyclotron accelerator where 60 MeV proton energy was used. The device received 100 krad at a dose rate of 1.3 krad/min and 900 krad at a dose rate of 13 krad/min. Gould-2 was exposed to  $Co^{60}$ , receiving a total dose of 3 Mrad at a dose rate of 3 krad/min. The irradiation was stopped for 1 hour after 100 krad to observe relaxation. Relaxation was observed for 9 hours after 1 Mrad, for 15 hours after 2 Mrad and for 12 hours after 3 Mrad. Gould-3 received a dose of 1 Mrad at a dose rate of 3 krad/min and was observed for 14 hours of relaxation. Gould-4 was tested for sectional  $Co^{60}$  irradiation (0.5" sections of the device were irradiated consecutively). The device was masked by 4" thick lead bricks with a 0.5" slit between them.

The ETEK device was supplied by E-TEK Dynamics Inc. ETEK-1 was exposed to  $\text{Co}^{60}$  receiving a dose of 1 Mrad at a dose rate of 3 krad/min. The relaxation of the device was observed for 12 hours.

The test apparatus used for in-situ measurements of the isolation and excess loss of the WDMS was modified and improved between tests. Figure 1 shows the method used which was preserved for all tests. The lasers were changed to cooled power stabilized laser diodes after the first test. ML-1 was the first device that was tested, and laser diodes at 1300 nm and 1547 nm were used. All of the other devices except for the ETEK were tested at 1306 nm and 1547 nm. The ETEK device was only tested in-situ at 1547 nm. Measurements at 1306 nm for the ETEK device were made only before and after irradiation. The laser intensity used varied from 1  $\mu\text{W}$  to 100  $\mu\text{W}$ . Enhanced annealing was not observed in photo bleaching tests at 1 mW optical power at both wavelengths.

One major modification that was made after all the ML devices and the first Gould device were tested was to add polarization control to both wavelengths. At 1547 nm, a motorized rotation stage was used to rotate a half-wave plate. At 1306 nm a manual rotation stage was used. This allowed us to measure, in-situ, the polarization properties of the WDM at 1547 nm, and to measure the polarization properties of the WDM at 1306 nm before and after irradiation.

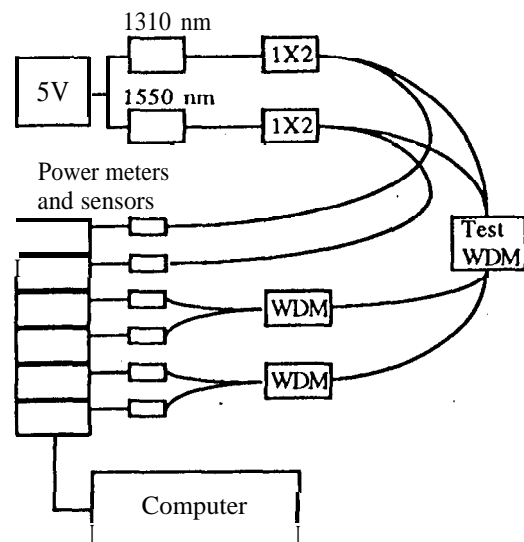


Fig. 4 Diagram of the experimental method used.

Figure 5 illustrates the method used in these experiments to be able to measure isolation and excess loss simultaneously at two wavelengths. Light at 1310 nm is injected into one of the input fibers of the test WDM, and light at 1550 nm into the other. The test WDM is then used as a multiplexer (see figure 1 a.) and combines most of the light at both wavelengths into one of the output fibers. The remaining light at 1310 nm and 1550 nm comes out of the other output fiber. Two WDMS are used to demultiplex (see figure 1 b.) the two wavelengths at each of the output fibers of the test WDM. Six optical power

sensors are used to track the two reference fibers and the four outputs of the WDM (two at each wavelength).

A measurement resolution in the crosstalk better than 0.01 dB was achieved by averaging over ten evenly spaced polarization states once the polarization control was in place.

## V. EXPERIMENTAL RESULTS

Table 1 gives the measured isolation before irradiation and the change induced by the radiation for all the tests that were done under the four columns labeled "ISOLATION (dB)". The change in isolation is given under the columns labeled " $\Delta\text{rad}$ ". The principal effect of radiation on the WDMS that were tested was to change their isolation. No significant changes in the excess loss of the device were observed. (Resolution in the measurement of the output of the WDM was better than 0.1 dB.)

The most important result from our experiments is that devices cannot be directly compared. Even the Gould devices, which were matched in isolation to better than 0.5 dB at 1311 nm and 1553 nm by the manufacturer, had different isolations at our wavelengths (1306 nm and 1547 nm) and had radically different isolation changes with radiation (see Table 1). The largest change in isolation was on ML-1 which changed by 10 dB at 1547 nm after 1 Mrad of 6 MeV protons. The isolation was observed to improve for ML-3 at both wavelengths and for Gould-2 at 1310 nm.

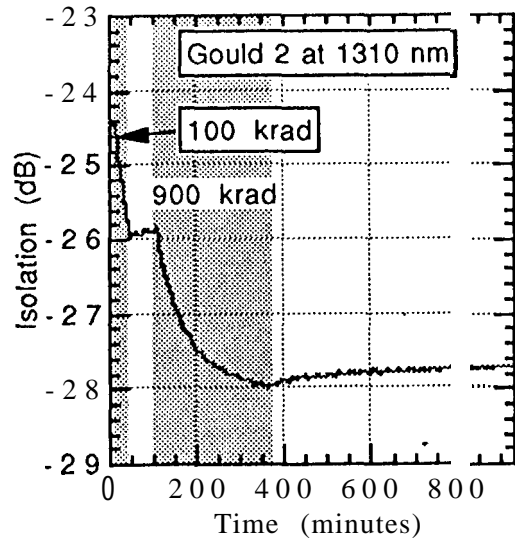
Figure 5 shows a sample of the data that was recorded. This data is for Gould-2 and shows the improvement in isolation at 1306 nm. The shaded regions mark the time when the radiation source was exposed. The white regions show the annealing in isolation after radiation.

The results from relaxation observations were qualitatively consistent with annealing of attenuation for SMF28 fiber [31]. Less than 20% of the total change in isolation annealed with a time constant of a few hours.

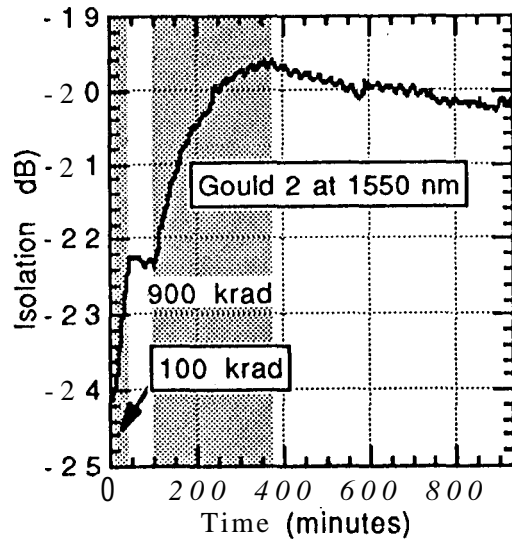
Sectional irradiations of ML-3 and Gould-4 give preliminary results on a very important type of experiment. Sectional irradiations give information on the sensitivity to radiation of the different regions of the device. It is observed that the center region is most sensitive, and that the input and output regions are only sensitive when close to the center of the device. These results, and results of future experiments will help in better understanding the physical mechanisms that result in an interaction between radiation and the electric fields in a WDM.

Table 1 includes the dependence on polarization for the ETEK device, which was found to be very sensitive to polarization. Only two orthogonal polarizations are shown, but it is clear that polarization is an issue for some of these devices. The polarization sensitivity of one of the ML WDMS was measured, and it was about the same as the ETEK. The polarization sensitivity of the Gould devices was measured and varied between 0.1 dB and 1.1 dB. Detailed results of the polarization measurements are not included here due to lack of space, but will be discussed at the SPIE conference in San Diego and in future publications. Since environmental

changes vary the birefringence of single mode optical fiber, **not controlling the polarization results in increased noise and drift in the isolation of the device.** Small changes in the excess loss (cO, 1 dB) are also known to be related to changes in polarization.



(a)



(b)

Fig. 5 Isolation changes with radiation (gray areas) and relaxation (white areas) for Gould-2 at (a) 1306 nm and (b) 1547 nm.

## VI. THEORETICAL ANALYSIS

### A. Rationale

Previous measurements on irradiated Ge-doped silica core fiber [1-5] indicate the presence of four types of color centers in irradiated Ge-doped silica. These are the Ge(1,2,3) and Ge-E' centers with absorption bands at 281 nm, 213 nm, 240 nm,

and 517 nm respectively. By [the Kramers-Kronig relation [28], the index of refraction (real part of the susceptibility function) is directly related to the absorption (imaginary part of the susceptibility function), so that the color centers in Ge-doped silica also affect its index of refraction. It can be shown the index increases for wavelengths greater than the absorption wavelength (normal dispersion) and decreases for wavelengths that are smaller (anomalous dispersion). Therefore, radiation will increase the index of the Ge-doped cores in SMF28 fiber at 1310 nm and 1550 nm.

The increase in index in the cores of the fibers will affect the coupling of the fused biconical tapered WDM studied in this paper. As can be seen in figure 3, the change in index in the cores will affect the antisymmetric mode more than the symmetric mode, since the magnitude of the electric field in the core region is greater for the antisymmetric mode. The difference in velocity between the two modes will decrease, changing the phase shift between the two modes at the end of the coupling region. As will be shown in the more detailed analysis that follows, the effect will be a positive shift in wavelength of the isolation vs. wavelength curve.

### B. Model

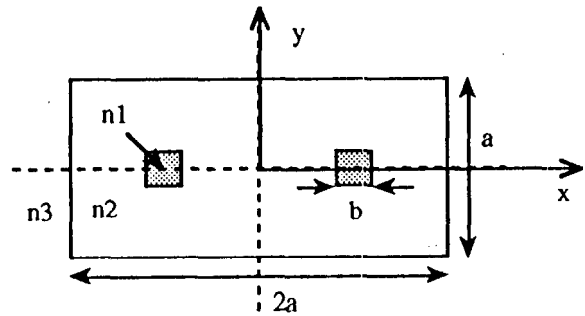


Fig. 6 Diagram of the rectangular dielectric waveguide used to model the coupling region of a WDM.

The most commonly used model for a fused biconical tapered coupler ignores the coupling in the taper regions and approximates the coupling region by a rectangular dielectric waveguide as shown in figure 6. When this simple structure is assumed, the coupling constants for both polarizations can be easily calculated by using equation (3). The coupling constants for x and y polarized modes in the rectangular dielectric waveguide are given from [17] by:

$$C_x + C_y = \frac{3\pi\lambda}{32n_2a^2} \left[ \frac{1}{\left(1 + \frac{1}{V}\right)^2} + \frac{1}{\left(1 + \frac{n_3^2}{n_2^2} \cdot \frac{1}{V}\right)^2} \right] \quad (4)$$

$$C_x - C_y = \frac{3\pi\lambda}{16n_2a^2} \cdot \frac{1}{V} \left( 1 - \frac{n_3^2}{n_2^2} \right) \quad (5)$$

where  $n_2$  is the index of the cladding,  $n_3$  is the index of the surrounding medium (typically air),  $a$  is the height of the rectangular cross-section as seen in figure 6, and:

$$V = \frac{2\pi a}{\lambda} (n_2^2 - n_3^2)^{1/2} \quad (6)$$

The analysis resulting in equations (4) and (5) ignores the cores of the fibers. These are shown as shaded squares in figure 6. In order to model the effects of a change in the index of refraction of the core, the effect of core index on the coupling constant needs to be calculated. This will be done by approximating the change in the effective indices of the symmetric and antisymmetric modes with an overlap integral calculation,

Marcatili solved for the modes of a rectangular dielectric waveguide [27]. We are only concerned about the first two fundamental modes which are the  $E_{11}^{x,y}$  (symmetric) and  $E_{21}^{x,y}$  (antisymmetric) linearly polarized modes. (These two modes are really TM modes with very small electric field in either the x or y direction.) Since the difference in index between the air and the cladding is so large, these two modes are tightly confined in the coupling region, and we can approximate the electric field inside the fiber as:

$$E_S^{x,y} = E_0 \cdot \cos\left(\frac{\pi x}{2a}\right) \cdot \cos\left(\frac{\pi y}{a}\right) \quad (7)$$

$$E_A^{x,y} = E_0 \cdot \sin\left(\frac{\pi x}{a}\right) \cdot \cos\left(\frac{\pi y}{a}\right) \quad (8)$$

where  $E_S$  is the electric field for the symmetric mode and  $E_A$  is the electric field for the antisymmetric mode. The effective index of each mode is given by the overlap integral of the square of the electric field and the index of refraction shown in figure 9:

$$n_{eff} = n_2 + (n_1 - n_2) \frac{\int_{-\frac{a+b}{2}}^{\frac{a+b}{2}} dx \int_0^{b/2} dy \cdot |E|^2}{\int_{-\frac{a-b}{2}}^{\frac{a-b}{2}} dx \int_0^{a/2} dy \cdot |E|^2} \quad (9)$$

where  $n_1$  is the index of refraction of the core and  $b$  is the width of the core in the model shown in figure 6.

Using equations (7), (8) in equation (9), we can calculate the change in the symmetric and antisymmetric indices of refraction caused by the cores of the fibers:

$$\Delta n_S = (n_1 - n_2) \cdot \frac{b}{a^2} \left[ b + \frac{a}{\pi} \sin\left(\frac{\pi b}{a}\right) \right] \quad (10)$$

$$\Delta n_A = (n_1 - n_2) \cdot \frac{1}{a^2} \left[ b + \frac{a}{\pi} \sin\left(\frac{\pi b}{a}\right) \right]^2 \quad (11)$$

We can use equation (3) together with equations (10) and (11) to solve for the change in the coupling constant caused by the difference between the core and cladding indices of refraction. The final result is a correction of equation (4) when the core index is taken into account:

$$C_x + C_y = \frac{3\pi\lambda}{32n_2a^2} \left[ \frac{1}{\left(1 + \frac{1}{V}\right)^2} + \frac{1}{\left(1 + \frac{n_2}{2} \cdot \frac{1}{V}\right)^2} \right] + 2 \cdot \Delta C \quad (12)$$

where,

$$\Delta C = \frac{2(n_1 - n_2)}{\pi\lambda} \cdot \sin\left(\frac{\pi a}{b}\right) \left[ \frac{\pi a}{b} + \sin\left(\frac{\pi a}{b}\right) \right] \quad (13)$$

Since the electric field profile is the same for the x-polarized and y-polarized modes, the change in the coupling constant is independent of polarization, so equation (5) does not change.

### C. Change in index at 1310 nm and 1550 nm

Hand and Russel [5] measured the effects of high intensity UV (488 nm) irradiation on the core index change of Ge-doped fiber. We are not aware that any similar measurements have been made for Co<sup>60</sup> or proton irradiation. Therefore, we will use the results from Hand and Russel to give a rough estimate of the core index change in SMF28 fiber after a 1 Mrad dose of radiation.

By using a three term Sellmeier expression, Hand and Russel predict a core index change of  $1.9 \cdot 10^{-4}$  at wavelengths greater than 1  $\mu\text{m}$  for a Ge-doped fiber with a radiation induced absorption of the order of 1000 dB/km at 488 nm. Assuming a Gaussian absorption lineshape for the Ge(1) color center absorption at 281 nm, and a linewidth of 1.97 eV [1], an absorption of 1000 dB/km at 488 nm corresponds to an absorption of 12.6 dB/km at 1300 nm. This is in excellent agreement with the measured absorption of SMF28 fiber exposed to Co<sup>60</sup> after a dose of 1 Mrad at 50 degrees Celsius [3].

It is therefore a reasonable assumption that the core index change for SMF28 fiber due to a dose of radiation of 1 Mrad is in the order of  $10^{-4}$  at 1310 nm and 1550 nm.

### D. Comparison with experimental results

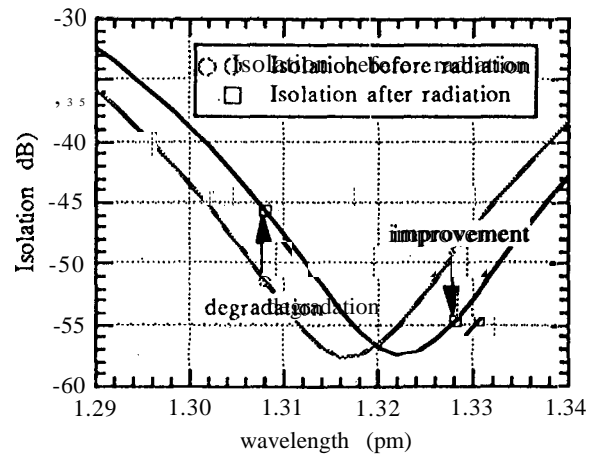


Fig. 7 Plot of equation (14) before and after core index change of  $10^{-4}$ .

Using equations (12) and (13), the change in the coupling constant due to a change in the index of the core can be easily calculated. Figure 7 shows the isolation as a function of wavelength before and after irradiation for a coupler with:

$$a = 15 \mu\text{m}$$

$$n_3 = 1$$

$$n_2 = 1.458$$

$$a/b = 9/125$$

The length of the coupler was 6,9 mm in order to locate the maximum and minimum coupling near 13,10 nm and 1550 nm before radiation. The maximum isolation predicted by the theory is too high since the excitation of higher order modes [23] and the effect of normal mode loss [7] are ignored. The change in core index caused by the radiation is assumed to be  $10^{-4}$ .

According to the model, radiation causes a red-shift in the isolation vs. wavelength curve. This result is in agreement with our experimental observations.

In the experiment, isolation improved in some devices, and degraded in others. As shown in figure 7, if the wavelength of the laser used to test the device is longer than the wavelength of maximum isolation, a red-shift of the isolation curve will improve the observed isolation. If, on the other hand, the probing wavelength is shorter than the wavelength of maximum isolation, radiation will degrade the isolation of the WDM.

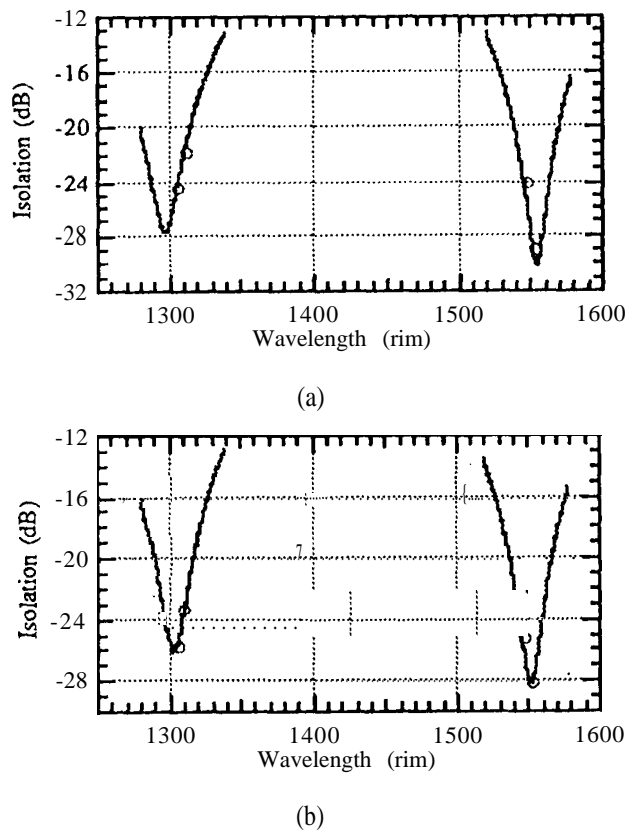


Fig. 8 Sinusoidal fit to pre-rad isolation data for (a) Gould-2 and (b) Gould-3

In order to make some correlation between the relative position of the laser wavelength and the direction of isolation

change with radiation, a sinusoidal fit to four data points was used to locate the position of the laser wavelength in the isolation curve. The results are shown in figure 8. Two of the data points (at 1311 nm and 1553 nm) were given by the manufacturer, and the other two are from our experimental measurements (at 1306 nm and 1547 nm). The fits are not exact since there is a range of error on each data point of approximately 0.3 dB due to the polarization dependence of isolation. Nevertheless, it is seen that the laser wavelength is shorter than the wavelength of maximum isolation for both devices at 1550 nm. Table 1 shows that the isolation decreased for both WDMs after radiation. Gould-2's isolation at 1306 nm improved, and the fit shows that the laser wavelength (the leftmost data point) is to the right of the isolation peak. Gould-3 degraded in isolation at 1306 nm, and the laser wavelength is nearly at the peak of isolation. Such fits were done for all four Gould devices, and the results were consistent with the direction of isolation change in the experiment.

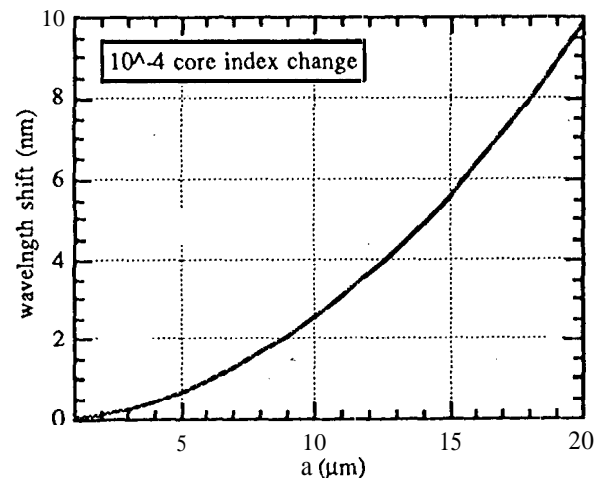


Fig. 9 Dependence of wavelength shift on dimensions of the coupling region.

Numerically, the shift in wavelength caused by the change in coupling can also be calculated. Figure 9 shows the dependence of the wavelength shift at 1310 nm on the dimensions of the coupling region. Typical dimensions of these devices range between 15  $\mu\text{m}$  and 20  $\mu\text{m}$ , so the corresponding wavelength shifts range between 6 nm and 10 nm. The shift in wavelength at 1550 nm is slightly smaller.

The results from sectional irradiations on ML-3 and Gould-4 indicate that parts of the taper region are also sensitive to radiation. This would be expected since there is some coupling between the two fibers in the taper regions. A complete calculation of the coupling in fused biconical tapered couplers may be useful to accurately model the effects of radiation, but such a detailed analysis was considered to be detrimental in providing a fundamental understanding of the problem.

As was mentioned in the last section, it appears that protons may induce a larger index change in these couplers than gamma-rays. It is possible that another mechanism for changing the index of refraction of the cores, unrelated to color center absorption, is the formation of permanent electric dipoles in the ionization trails of the protons [5]. This frozen-in electric fields could generate localized refractive index changes by means of the electro-optic effect.'

## VII. CONCLUSION

The effects of  $\text{Co}^{60}$  and proton irradiation of fused biconical taper wavelength division multiplexers for 1310 nm and 1550 nm have been investigated. Changes in the excess loss of these devices is less than 10<sup>-4</sup> dB/krad, while changes in isolation as large as 10<sup>-2</sup> dB/krad were measured. A theoretical model indicates that the change in isolation may be caused by radiation-induced index changes in the coupling region. These index changes produce a red-shift in the isolation characteristics of the WDM of approximately 10 nm.

Eight separate devices from three different manufacturers were tested in a total of twenty two irradiations. The results from straight irradiations, annealing at room temperature after radiation, and sectional irradiation of two WDMS were described. In addition, measurements on the effect of polarization on isolation of six WDMS and a comparison between proton and  $\text{Co}^{60}$  were briefly discussed,

The manufacture of these devices could be tailored so that the isolation improves when exposed to radiation. Our theory also suggests that a WDM with a shorter and narrower coupling region may be less sensitive to radiation. These factors should be taken into account in the development of a radiation hard fused biconical taper WDM. Other devices that may be similarly affected by radiation include tapered waveguide optical filters, fused biconical taper polarization splitters, and evanescently coupled devices.

The authors thank Simon Cao at E-TEK and Matt McLandrich at NCCOSC for donating devices for these tests.

## VIII. REFERENCES

- [1] E.J. Friebele and D.L. Griscom, "Color Centers in Glass Optical Fiber Waveguides", Mat. Res. Symp. Proc. 61 (1986)
- [2] V. II. Neustruev et al, "UV and Gamma Induced Colour Centres in Germanium-doped Silica Glass and Fibers", SPIE 992 Fiber Optics Reliability: Benign and Adverse Environments II (1988)
- [3] E.J. Friebele, M.E. Gingerich, and D.L. Griscom, "Survivability of optical Fibers in Space", SPIE 1791 Optical Materials and Testing: Benign and Adverse Environments (1992)
- [4] B. Male, et al, "Ultraviolet Light Photosensitivity in Ge-doped Silica Fibers: Wavelength Dependence of the Light-induced Index Change", Opt. Lett. 15, 17 (1990)
- [5] D. P. Hand, and P. S. J. Russell, "Photoinduced Refractive-index Changes in Germanosilicate Fibers", Opt. Lett. 15, 2 (1990)
- [6] Michel Dignonnet and H.J. Shaw, "Wavelength multiplexing in single-mode fiber couplers", Appl. Opt., 22,3 (1983)
- [7] Robert C. Youngquist, Loren F. Stokes, Herbert J. Shaw, "Effects of Normal Mode Loss in Dielectric Waveguide Directional Couplers and Interferometers", IEEE J. Quantum Electron., QE-19, 12 (1983)
- [8] Yariv, Amnon, *Introduction to Optical Electronics*, 3d Ed. New York: Holt Rinehart and Win.. [on Inc., 1985.
- [9] Marcuse, Dietrich, *Theory of Dielectric Optical Waveguides*. New York: Academic Press. 1974.
- [10] H.F. Schlaak, "Modulation Behaviour of Integrated Optical Directional Couplers", J. Opt. Comm., 5,4 (1984)
- [11] E. W. Taylor, "Radiation Effects in Guided Wave Devices", SPIE 1794 Integrated Optical Circuits II (1992) pp 54-61
- [12] E. W. Taylor, "Behaviour of Coupled Waveguide Devices in Adverse Environments", SPIE 1314 Fibre Optics (1990) pp 155-167
- [13] E. W. Taylor, "Ionization-Induced Refractive Index and Polarization Effects in LiNbO<sub>3</sub>:Ti Directional Coupler Waveguides", J. Lightwave Tech., 9,3 (1991) pp 335-40
- [14] D. R. Moore, "Reliability Testing of Fused Couplers", SPIE 988 Components for Fiber Optic Applications and Coherent Lightwave Communications (1988) pp 27-33
- [15] G. Winzer, "Wavelength Multiplexing Components--A Review of Single-Mode Devices and Their Applications", J. Lightwave Tech., LT-2, 4 (1984) pp 369-78
- [16] H. Ishio, J. Minowa, and K. Nosu, "Review and Status of Wavelength-Division-Multiplexing Technology and Its Application", J. Lightwave Tech., LT-2, 4 (1984) pp 448-63
- [17] F. P. Payne, C. D. Hussey, and M. S. Yataki, "Polarisation Analysis of Strongly Fused and Weakly Fused Tapered Couplers", Electron. Lett., 21, 13 (1985) pp 561-3
- [18] A. Ankiewicz, A. W. Snyder, X. H. Zheng, "Coupling Between Parallel Optical Fiber Cores--Critical Examination", J. Lightwave Tech., LT-4,9(1986) pp 1317-23
- [19] F. P. Payne, C. D. Hussey, and M. S. Yataki, "Modelling Fused Single-Mode-Fibre Couplers", Electron. Lett., 21, (1985) pp 461-2
- [20] J. D. Love, M. Hall, "Polarisation Modulation in Long Couplers", Electron. Lett., 21, 12 (1985) pp 519-21
- [21] A. W. Snyder, "Polarizing Beamsplitter from Fused-Taper Couplers", Electron Lett, 21, 14(1985) pp. 623-5
- [22] J. V. Wright, "Wavelength Dependence of Fused Couplers", Electron. Lett., 22,6 (1986) pp. 320-1
- [23] M. Eisenmann and E. Weidel, "Single-Mode Fused Biconical Couplers for Wavelength Division Multiplexing with Channel Spacing between 100 and 300 nm", J. Lightwave Tech., 6, 1 (1988) pp 113-9
- [24] H. Henschel, O. Kohn, and H. U. Schmidt. "Radiation sensitivity of fibre optic couplers", SPIE 1791 Optical Materials Reliability and Testing (1992) pp 151-63
- [25] M. Bertolotti, et al, "Radii and refractive index changes in  $\gamma$ -irradiated optical fibres", Rad. Effects. Lett., 43 (1979) pp 177-80
- [26] V. J. Tekippe, "Passive Fiber Optic Components Made by the Fused Biconical Taper Process", SPIE 1085 Optical Fibers and Their Applications (1990)
- [27] E. A. J. Marcatili, "Dielectric Rectangular Waveguide and Directional Coupler for Integrated Optics", Bell Sys. Tech. J., 48, (1969) pp. 2071-2102
- [28] Yariv, Amnon, *Quantum Electronics* 3d Ed., New York: John Wiley & Sons, Inc., 1989